

# Measurement of the adhesion of a brittle film on a ductile substrate by indentation

BY M. D. DRORY<sup>1</sup> AND J. W. HUTCHINSON<sup>2</sup>

<sup>1</sup>*Crystallume, 3506 Bassett Street, Santa Clara, CA 95054, USA*

<sup>2</sup>*Division of Applied Sciences, Harvard University, Cambridge, MA 02138, USA*

The indentation of a brittle film on a ductile substrate is analysed for obtaining the interface toughness. This measurement method of adhesion provides a simple technique for sampling a small area of the interface on practical geometries with common laboratory equipment. Mechanics solutions are presented to access the interface toughness,  $\Gamma_c$ , from measurements of the applied load, delamination radius, film thickness and film–substrate material properties. The test is found to be particularly effective for films under large residual compression. Measurements of the interface toughness ( $\Gamma_c \sim 45 \text{ J m}^{-2}$ ) are made for a diamond-coated titanium alloy.

---

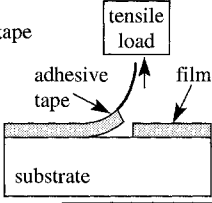
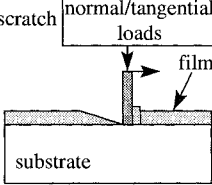
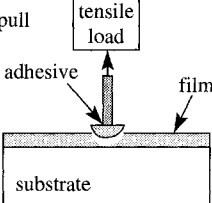
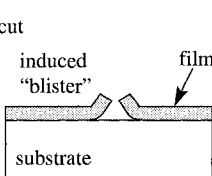
## 1. Introduction

Many modern engineering applications require advances in materials to simultaneously meet several practical design functions. For example, structural ceramics have long been sought for elevated temperature use at greater than 1200 °C in aerospace propulsion systems. These substrate materials are often used in conjunction with *coatings* to enhance reliability, such as chemical resistance in aggressive environments, wear resistance in contact loading applications and thermal barriers in locations which exceed the use temperature of the substrate. Failure of the coating in these instances leads to catastrophic failure of the structural component, motivating considerable interest in recent years for providing fail-safe designs of coatings as an integral component of the engineering system (Evans *et al.* 1988).

The fracture modes of coatings have been considered in detail by Hutchinson & Suo (1991), and are characterized by splitting of the coating, delamination and the ancillary problem of substrate failure near the interface. These events are largely motivated by residual film stresses that arise during coating deposition, but may also be the result of ‘in-service loading’ such as that developing with mechanical contact. As elaborated in subsequent sections, the sign and magnitude of residual film stresses is a central consideration in the mechanical reliability of coatings. This is due to the differences in mechanical response which coatings exhibit, whether compressive or tensile stresses, and as a result of the very large magnitude of these stresses which may be present.

The aspect of film reliability explored here is the measurement of adhesion for brittle coatings under compressive stresses on relatively ductile substrates. Adhesion measurement of thin diamond-coatings on a titanium metal alloy will be the practical focus for comparison with the mechanics analysis provided in the present work.

Table 1. Selected adhesion measurement techniques, where  $T$  denotes tensile stress and  $C$  compressive stress

test technique	schematic	characteristic aspect for film delamination	limitations on specimen geometry	measurement of interface fracture toughness	sign of film stress	film	substrate	comments
1 tape		tensile force	none	no	T/C	ductile	ductile/ brittle	analysis is complex; not for brittle films
2 scratch		sliding penetrator	none	no	T/C	ductile	ductile/ brittle	analysis is complex; not for hardcoatings
3 pull		tensile force	none	no	T/C	ductile	ductile/ brittle	strength measurement
4 cut		residual film stress	none	yes	T	ductile/ brittle	ductile/ brittle	precracking difficult for hardcoatings; limited range of interface toughness

The extreme properties of diamond (e.g. hardness, stiffness) provide a considerable challenge for adhesion testing, and illustrate aspects of this topic for hard coatings which are of wide practical importance.

The need to distinguish the sign of the film stress and the deformation characteristics of the substrate (ductile versus brittle) are central issues in the behaviour of various test procedures; several tests are illustrated in table 1. These procedures involve inducing film delamination in a controlled manner as to allow for a quantitative measurement of adhesion. However, as elaborated below, important distinctions can be made for the robust nature of each test and the applicability of the adhesion measurement in design and reliability calculations. It appears that all testing methods are limited to some envelope of material properties and testing conditions. No single test method provides useful information for all combinations of film and substrate materials.

Commonly used tests for evaluating adhesion are performed by inducing delamination by the following means (table 1): (1) lifting the film with the aid of an adhesive tape; (2) spalling a portion of the film by scribing the surface with a diamond probe (scratch test); and (3) removing the film by pulling an adhesively mounted rod with

Table 1. *Cont. Selected adhesion measurement techniques*

test technique	schematic	characteristic aspect for film delamination	limitations on specimen geometry	measurement of interface fracture toughness	sign of film stress	film	substrate	comments
5 four-point bending		select mixed-mode loading	yes (special geometry)	yes	T/C	ductile	ductile/ brittle	pre-cracking difficult; involved specimen preparation
6 blister		film pressurization	yes (special geometry)	yes	T	ductile	ductile/ brittle	complex specimen preparation and pre-cracking
7 indentation-sharp penetrator		substrate plasticity (induced residual stress)	yes (requires smooth interface)	yes	T/C	ductile/ brittle	ductile/ brittle	requires smooth surface; for limited interface toughness
8 indentation-blunt penetrator		substrate plasticity (induced residual stress)	none	yes	C	brittle	ductile	for ductile substrates

a tensile force (table 1, nos. 1–3). In each case, a measure of adhesion is attempted by relating it to the forces applied to the tape (Kinloch *et al.* 1994), diamond probe (Perry 1983), or rod at the onset of delamination (Steinmann & Hintermann 1989). These methods are commonly used in the evaluation of polymer and other highly pliable coatings, but have limited usefulness for adhesion measurement of brittle films. In the latter case, film splitting is prevalent and greatly reduces the applied force (energy) directed towards delamination. Other difficulties include the large sensitivity of the scratch and pull tests to the applied force vector. The scratch test is hampered in examining coatings of extreme hardness (such as diamond, TiC, TiCN) by erosion of the probe (Jindal *et al.* 1987).

The ‘cut’ test is an adhesion test which relies on large residual (tensile) film stresses to promote delamination (table 1, no. 4). It is also adversely effected by the extreme hardness of diamond coatings. A critical aspect of this test requires splitting the film (by scribing, or other methods) with the anticipation of crack extension along the film–substrate interface. The interface in this case is the plane of weakness in contrast to the splitting mode of failure of the film. Difficulties arise in scribing hardcoatings such as diamond, which are also most commonly in a state of compression.

Another practical aspect of adhesion measurement is illustrated in difficulties aris-

ing from the use of sample 'coupons', such as those associated with a four-point bending method (table 1, no. 5). In this technique, accurate values of the interface toughness can be obtained by precracking a coated bending beam specimen and monitoring the onset of delamination with increasing (bending) load (Charalambides *et al.* 1990). Practical issues arise with this and other tests which require the fabrication of special coupons. For example, testing of the adhesion of hardcoatings on tool inserts of cemented carbide by this method requires substrates of a different geometry (and size) than the actual component. The chemistry of the coupon substrate and interface may differ considerably from the tool insert. Adhesion measurement of the specific interface (and substrate) of interest is needed where a size dependence in material properties is evident (typically relating to processing methods).

Accurate measurements of film adhesion can also be made with the special geometry of the bulge test (table 1, no. 6), in which delamination occurs by pressurizing the film from an etched (or otherwise machined) opening in the substrate (Sizemore *et al.* 1995). The interface toughness can be derived from the film properties, hole size and pressure required to advance an interface crack. This test has the attractive feature that the delamination is self-limiting when the pressurization is produced by a fixed gas or liquid volume. As the film delaminates, the driving force diminishes. Catastrophic delamination often creates experimental difficulties, which is avoided by testing with a driving force which diminishes with increasing crack length. The current use of the test is restricted to films in tension to avoid complexities of film wrinkling associated with the buckling of films in compression. Considerable development for the etching processes is typically required for each substrate material of interest, particularly if small areas of the interface are to be examined. In this regard, adhesion measurements by indentation methods provides considerable promise because of its potential small probe size.

Film delamination (and a measure of the interface toughness) is obtained with indentation methods by penetration of the coating with a rigid punch. In some tests the penetrator only induces significant deformation in the film, while in others it produces plastic deformation in the substrate as well (table 1, nos. 7 & 8). The penetrator is typically a diamond pyramid with  $136^\circ$  included angles or a spherical diamond indenter of 200  $\mu\text{m}$  radius. In each case, the penetrator is used in conjunction with common procedures for hardness testing of materials. A Vicker's indenter is used in 'microhardness' testing, and a brale 'C' indenter is used in the Rockwell hardness test (Dieter 1986). A metal ball has also been used for measuring the adhesion of polymer coatings (Ritter *et al.* 1989). With each of these penetrator shapes, the purpose is to induce an axisymmetric region of delamination in the vicinity of the contact zone. The behaviour of the film (and substrate) in this region depends on the relative ductility of each material.

In the case of a relatively ductile material on a brittle substrate, delamination is induced by producing plastic deformation in the film, avoiding penetration of the substrate (Rossington *et al.* 1984). Delamination occurs by plastically induced stresses in the film near the contact region and takes place during *unloading* of a Vicker's indenter. Spalling may also accompany delamination in the presence of large compressive (residual) film stresses. This was considered by Rossington *et al.* (1984) for ZnO films deposited on a silicon substrate. The sharp (Vickers) penetrator in this experiment induces plastic deformation in the film without penetrating through the film to the substrate. Interaction with the substrate greatly complicates the analysis for extracting a quantitative measure of coating adhesion from this test.

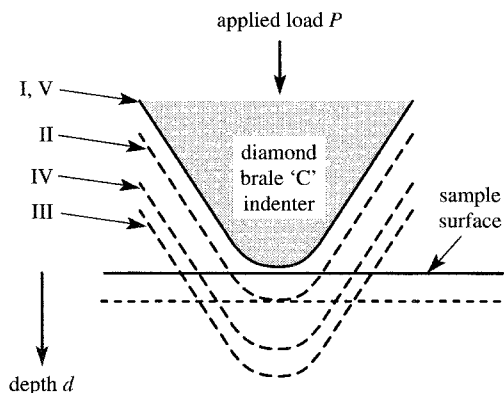


Figure 1. Schematic of the brale indentation test.

As the film hardness increases, the ability of the penetrator to induce a sufficiently large contact zone for delamination is diminished. For example, indentation testing of diamond films on brittle substrates (e.g. single crystal silicon) suggested that such delamination may be possible (Gamlin *et al.* 1991). However, subsequent work on the same system of materials indicated that with typical levels of adhesion between diamond and silicon, delamination is not achieved without applied indentation loads that result in failure of the diamond penetrator and severe damage of the substrate. It remains as a future topic of research to develop an adhesion test for this case; namely, a small probe of adhesion on the actual coated sample of interest where the film and substrate are each brittle (e.g. ceramic-ceramic systems).

The focus in the present work is in examining an indentation test of adhesion for a brittle film on a relatively ductile substrate. It involves the use of the diamond brale indenter (figure 1) under much greater loads than described previously for the Vicker's indentation tests, whereby plastic deformation of the *substrate* is encouraged. Film delamination proceeds as a result of the (relatively) gross deformation of the substrate. This method has been previously examined for a number of hardcoatings, such as TiC and TiCN, on cemented carbide tool inserts (Mehrotra & Quinto 1985) and on diamond-coated tool inserts (Yen *et al.* 1990). The load is applied by the use of the standard Rockwell Hardness Tester which is capable of supplying loads to nearly 1500 N. The use of this tester is a very attractive feature of the method because of its low cost and current widespread use in metallurgical laboratories. However, some consideration is required of the loading cycle associated with this hardness testing machine (figure 1).

Rockwell hardness is obtained in a different manner than microhardness using the Vicker's indenter. In the microhardness case, the load is applied continuously through a damping mechanism until a single value is achieved as determined by the use of a hanging weight system. The typical applied loads with microhardness testing are 10 to 200 N. In contrast, the Rockwell test applies a 100 N preload, followed by the major load (*ca.* 600–1500 N). The major load is applied and released automatically in a time-scale defined by the standard test procedure (ASTM 1994). Finally, the preload is manually released (figure 1). Although these loading steps are a complication in analyzing the adhesion test, it does enable one to use standard metallurgical laboratory equipment without modification. This is an important consideration for broad use of a testing method which transitions from the laboratory to production

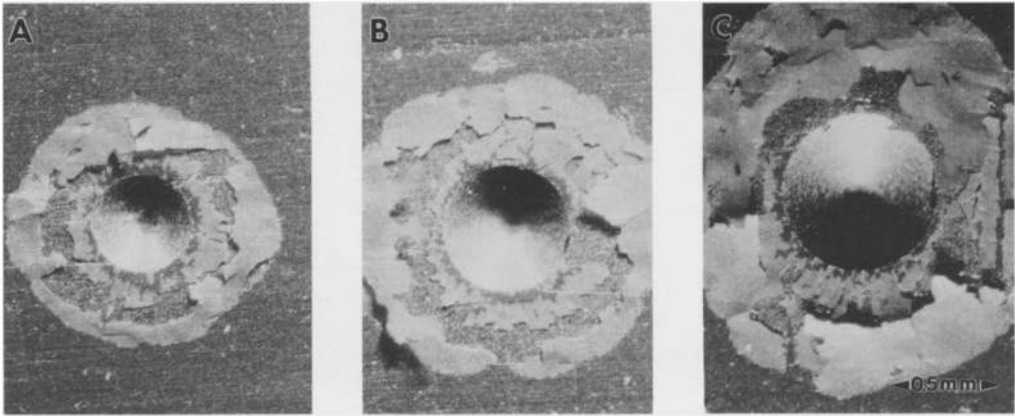


Figure 2. Brale indentation of diamond-coated titanium alloy at three loads: 688, 1079 and 1570 N.

environments, without the substantial costs commonly associated with low usage, novel testing equipment.

A common goal of this and other methods is useful information on adhesion through the measurement of a fundamental engineering parameter, such as the interface toughness,  $\Gamma_c$ . Previous mechanics analyses have been incomplete in extracting  $\Gamma_c$  from brale indentation results for a brittle film on a ductile substrate. We address these issues in this work in order to quantify the test method so as to obtain  $\Gamma_c$  for a range of practical cases. In describing the testing methods selected above, the limitations of each test were recognized; the limitations on the brale indentation test will be similarly described.

The brale indentation test is applied to a diamond-coated titanium alloy. Details of the film deposition are provided in §4. Examples of brale indentation for this system is provided in figure 2 where the axisymmetric delamination region is clearly visible beyond the contact zone for three indentation loads. Additional features of the damage region include film splitting and spalling. The task here is to provide a measure of the interface toughness as a function of the applied load, film thickness and residual stress, and material properties of diamond and the titanium alloy.

## 2. Surface strains due to conical indentation of an elastic–plastic substrate

The elastic energy in the film available to drive the interface delamination arises from two sources: initial residual stress and additional stress induced in the film in the vicinity of the indentation. The initial residual stress can be generated by thermal expansion mismatch between the film and the substrate, as intrinsic stresses associated with the deposition process, or as some combination of the two. Here we will restrict attention to residual stresses which are uniform through the thickness of the film and equi-biaxial such that the in-plane stress components are  $\sigma_{xx} = \sigma_{yy} = \sigma_0$ . As long as the film remains attached to the substrate, it is forced by the indenter to displace radially in its own plane, and this is the primary contribution to the elastic energy in the film resulting from indentation. The film also experiences some out of plane bending due to the vertical deflection of the substrate surface induced by the indenter. It will be shown that the elastic energy stored in bending is negligibly

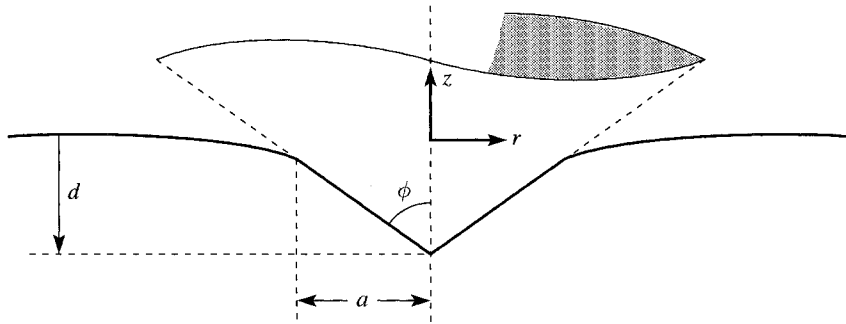


Figure 3. Axisymmetric geometry of indentation experiment for mechanics analysis.

small compared to that stored in in-plane straining when the indentation depth is large compared to the film thickness, which is the case of interest here.

For films that are very thin compared to the depth of indentation into the substrate, the film has little effect on the deformation of the substrate by the indenter and is forced to displace with the surface of the substrate, assuming it remains attached. For the diamond–titanium system discussed later, the indentation depth is between one hundred and one thousand times the film thickness. Thus, the essential information needed to carry out a delamination analysis of the film is the radial surface displacement of an elastic-plastic half space loaded by a conical indenter. Numerical solutions to such indentation problems have recently become available (e.g. Bower *et al.* 1993). Here, we make use of surface displacements of a half-space due to a conical indenter with a  $60^\circ$  semi-angle computed using the program developed by N. Ogbonna & N. A. Fleck (Cambridge University, personal communication). Specifically, the radial surface displacement will be used to generate the strains induced in the attached film due to indentation. When combined with residual strains present in the film prior to indentation, these results permit the determination of the energy release rate available to drive an axisymmetric interface crack expanding outward from the indentation. The relevant results for the attached film will be presented in the remainder of this section. The determination of the energy release rate is addressed in §3.

#### (a) Displacements and strains

The substrate half-space is modelled as a finite strain,  $J_2$  deformation theory solid characterized by a Ramberg–Osgood true-stress–logarithmic-strain curve in uniaxial tension which is given by

$$\varepsilon = \frac{\sigma}{E_s} + \frac{3}{7} \frac{\sigma_Y}{E_s} \left( \frac{\sigma}{\sigma_Y} \right)^{1/N} \quad (2.1)$$

Thus, the material comprising the substrate is characterized by its Young's modulus  $E_s$ , Poisson's ratio  $\nu_s$ , tensile yield stress  $\sigma_Y$  and strain hardening exponent  $N$ . With reference to the axisymmetric geometry shown in figure 3, let  $r$  and  $z$  be the radial and axial coordinates of material points in their displaced positions,  $d$  be the depth of penetration relative to the remote surface of the substrate,  $\phi$  the semi-angle of the conical indenter and  $a$  be the radius of the indentation at the circle of points where the indenter and the surface make contact. The indenter surface is assumed to be frictionless. Let  $u^I(r)$  and  $w^I(r)$  be radial and vertical displacement components of points on the surface of the half-space. For a given semi-angle of the rigid

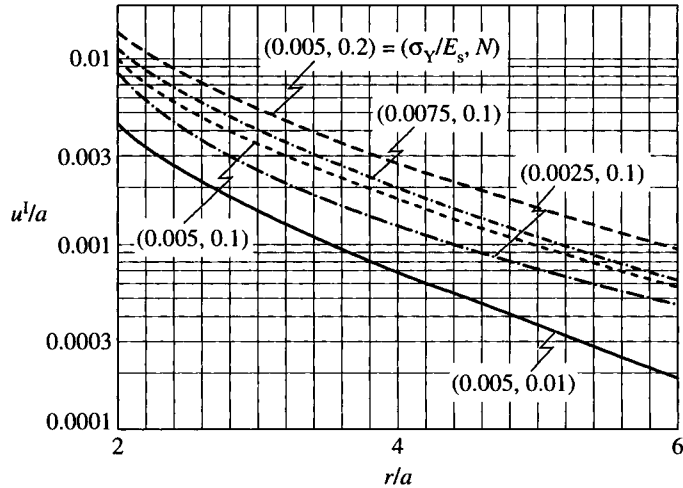


Figure 4. Radial component of the surface displacement of the substrate  $u^I$  vs distance from the indentation as function of the yield stress to Young’s modulus ratio, and work hardening exponent.

conical indenter, dimensional considerations dictate that the surface displacements must depend on dimensionless functions  $F_r$  and  $F_z$  according to

$$\frac{u^I}{a} = F_r \left( \frac{r}{a}, \frac{\sigma_Y}{E_s}, N, \nu_s \right) \quad \text{and} \quad \frac{w^I}{a} = F_z \left( \frac{r}{a}, \frac{\sigma_Y}{E_s}, N, \nu_s \right). \quad (2.2)$$

It will be shown that the strain energy due to bending in the film associated with the vertical displacement  $w^I$  is negligible when the indentation depth is large compared to the film thickness, and therefore results for  $w^I$  need not be presented. Plots of  $u^I/a$  as a function of  $r/a$  obtained from the numerical solution are shown in figure 4 for several combinations of  $\sigma_Y/E_s$  and  $N$ , all for  $\nu_s = 0.3$ ,  $\phi = 60^\circ$ . Far from the indenter, the displacement  $u^I$  must approach the elastic Boussinesq solution for a concentrated load  $P$  acting normal to the half-space,  $u = (1 + \nu_s)(1 - 2\nu_s)P/(2\pi Er)$ , where  $P \approx 3\sigma_Y\pi a^2$ . However, this limiting solution is only attained at distances from the indenter which are large compared to the range of interest in the present application.

For evaluating the influence of the indenter it is useful to have an analytical approximation  $u^I$ . The approximation is required to give a good fit of the numerical results in figure 4 over the range  $2 \leq r/a \leq 5$ , because this is the range of most interest for application to the delamination test. For  $r < 2a$ , the strains in the film induced by the indenter are sufficiently large that the delamination will almost certainly exceed  $2a$ . By contrast, it will be seen that indentation-induced strains will be insufficient to spread the delamination to distances beyond about 4 or  $5a$ . An accurate representation of the numerical results in figure 4 is achieved using a polynomial approximation of the form

$$\ln(F_r) \equiv \ln(u^I/a) = b_0 + b_1(r/a) + b_2(r/a)^2 + b_3(r/a)^3, \quad (2.3)$$

where the set of four coefficients of the polynomial are listed in table 2 for each of the five curves.

In the range  $2 \leq r/a \leq 5$ , the strains in the surface of the half-space are accurately related to the radial displacement by the small strain expressions. Thus, from (2.2),



Table 2. Coefficients for equation (2.3)

$N$	$\sigma_Y/E_s$	$b_0$	$b_1$	$b_2$	$b_3$
0.01	0.005	-2.1884	-2.1921	0.3287	-0.0239
0.1	0.005	-0.0398	-3.3853	0.6630	-0.0522
0.2	0.005	-0.7655	-2.4513	0.4130	-0.0300
0.1	0.0025	2.0424	-5.3558	1.1811	-0.0961
0.1	0.0075	-0.9206	-2.5083	0.4286	-0.0325

it follows that the radial and circumferential surface strains depend on  $r/a$  as

$$\epsilon_r^I = \frac{du^I}{dr} = F'_r \quad \text{and} \quad \epsilon_\theta^I = \frac{u^I}{r} = \frac{a}{r} F_r, \tag{2.4}$$

where the prime denotes a derivative with respect to  $r/a$ . These are the in-plane strains induced in the film by the indenter as long as the film remains attached to the substrate under the condition that the strains due to bending are small by comparison. Approximations to these strains are obtained using (2.3) in (2.4).

(b) *Distribution of stresses and elastic energy in film*

The above results are now used to generate distributions of the elastic energy stored in the film as a result of the combination of initial residual stress and indentation, assuming the film is attached to the substrate. Denote the film thickness by  $t$ . Assume the film is isotropic in its plane with  $E$  and  $\nu$  as the Young's modulus and Poisson's ratio governing in-plane stressing. Let  $\sigma_0$  and  $\epsilon_0$  be the uniform, equi-biaxial residual stress and strain in the film prior to indentation which are related by

$$\epsilon_0 = \frac{(1 - \nu)}{E} \sigma_0. \tag{2.5}$$

The total in-plane strains in the film are  $\epsilon_r = \epsilon_r^I + \epsilon_0$  and  $\epsilon_\theta = \epsilon_\theta^I + \epsilon_0$ . The stresses in the film are  $\sigma_r = [E/(1 - \nu^2)][\epsilon_r + \nu\epsilon_\theta]$  and  $\sigma_\theta = [E/(1 - \nu^2)][\epsilon_\theta + \nu\epsilon_r]$ . Distributions of the two stress components are illustrated in figure 5 in the form of  $\sigma_r/\sigma_0$  and  $\sigma_\theta/\sigma_0$  as a function of  $r/a$  for several levels of negative  $\epsilon_0$ . The radial stress  $\sigma_r$  is compressive and substantially larger in magnitude than the circumferential component; it falls to the remote level  $\sigma_0$  at values of  $r$  from 4 to 5 times the indentation radius. The circumferential component becomes tensile at distances less than about  $1.5a$ , depending on the residual compression in the film. When the film is in residual compression, or has a very small residual tension, an indenter will produce radial cracks in a brittle film only within a distance of about  $\frac{1}{2}a$ , at most, from the edge of the indentation. By contrast, the effect of the indenter on the radial stress is more pronounced, and delaminations spreading out to farther distances are possible.

Let  $\Omega$  be the elastic strain energy per unit area stored in the film due to the in-plane stresses, i.e.

$$\Omega = \frac{1}{2} \sigma_{ij} \epsilon_{ij} t = \frac{1}{2} \frac{Et}{(1 - \nu^2)} (\epsilon_r^2 + \epsilon_\theta^2 + 2\nu\epsilon_r\epsilon_\theta). \tag{2.6}$$

It follows from (2.4) that  $\Omega$  depends on indentation radius  $a$  and the radial coordinate

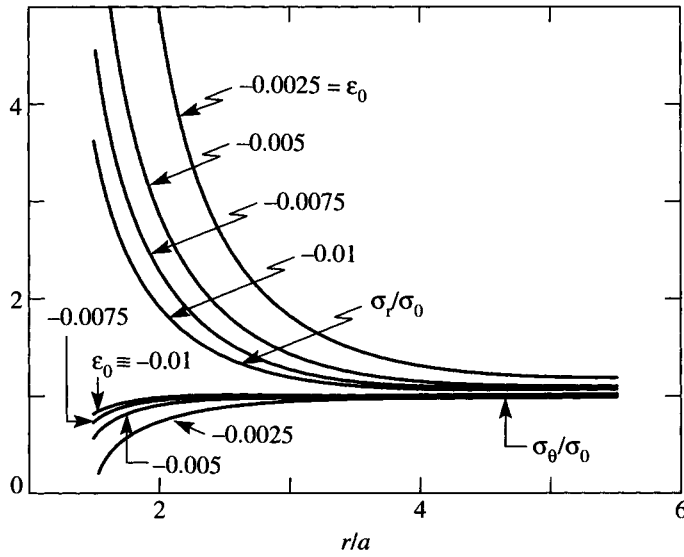


Figure 5. Variation in radial and circumferential components of film stresses with distance from the indentation.  $\nu_s = \nu = 0.3$ ,  $N = 0.1$  and  $\sigma_Y/E_s = 0.005$ .

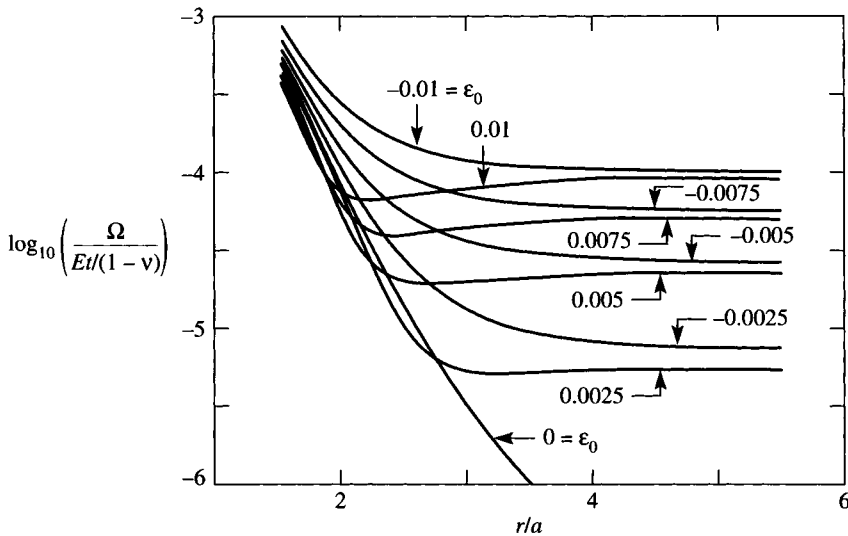


Figure 6. Normalized elastic strain energy per unit area as a function of residual film strain and distance from the indentation.  $\nu = 0.3$ ,  $\sigma_Y/E_s = 0.005$  and  $N = 0.1$ .

$r$  only through the combination  $r/a$ . Remote from the indenter ( $r/a \gg 1$ ), the strain energy in the film is due to the residual stresses alone and is given by

$$\Omega_0 = \frac{Et}{(1-\nu)} \epsilon_0^2 = \frac{(1-\nu)t}{E} \sigma_o^2. \tag{2.7}$$

Distributions of  $\Omega$  have been computed using (2.6) together with the approximations for the indenter strains given by (2.4) with (2.3). The plots in figure 6 employ the normalization  $\Omega/[Et/(1-\nu)]$  such that these curves depend on the choice of  $\sigma_Y/E_s$ ,  $N$ ,  $\nu_s$  and  $\nu$  but not on the film modulus  $E$  or its thickness. The curves in

figure 6 expose the fact that the indenter dominates the distribution for  $r < 2a$ . At distances from the indenter between about  $3a$  to  $5a$ , depending on the value of  $\varepsilon_0$ , a transition occurs with  $\Omega$  approaching the remote value  $\Omega_0$ . The indenter creates a steep variation in the distribution of elastic energy stored in the film with a drop-off which can be as large as a factor of 10 or 100 or even larger, depending on  $\varepsilon_0$ . There is a significant difference between the distributions for compressive and tensile residual strains. In the case when  $\varepsilon_0$  is negative the strain energy per unit area in the film falls monotonically with distance from the indenter. By contrast,  $\Omega$  drops below  $\Omega_0$  and then approaches this limit from below as  $r/a$  becomes large when  $\varepsilon_0$  is positive. The difference in behaviours is due to the fact that the radial strain component induced by the indenter is negative and substantially larger in magnitude than the circumferential component, thereby increasing the magnitude of the total radial component when  $\varepsilon_0$  is negative and diminishing it when  $\varepsilon_0$  is positive. For films with a compressive residual strain, the strong monotonic variation in  $\Omega$  induced by the indenter will be seen to give rise to interface delamination out to a well defined distance, making measurement of the toughness of the film-substrate interface feasible. The indentation test is not likely to be a good choice for this purpose when the residual strain is significantly tensile.

To see that the out-of-plane displacement  $w^I$  makes a negligible contribution to the energy in the film, consider the following estimate of the elastic bending energy per unit area induced in the film at  $r$ :

$$\frac{Et^3}{24(1-\nu^2)}(\kappa_r^2 + \kappa_\theta^2 + 2\nu\kappa_r\kappa_\theta),$$

where  $\kappa_r = d^2w^I/dr^2$  and  $\kappa_\theta = r^{-1}dw^I/dr$  are the curvatures induced in the film in the radial and circumferential directions. From (2.2), the bending energy per unit area is

$$\frac{Et(t/a)^2}{24(1-\nu^2)}\left(F_z''^2 + \left(\frac{a}{r}F_z'\right)^2 + 2\nu\frac{a}{r}F_z''F_z'\right), \tag{2.8}$$

where the prime again denotes differentiation with respect to  $r/a$ . When  $\varepsilon_0 = 0$ , the corresponding expression for  $\Omega$  is

$$\Omega = \frac{1}{2}\frac{Et}{(1-\nu^2)}\left(F_r''^2 + \left(\frac{a}{r}F_r'\right)^2 + 2\nu\frac{a}{r}F_r''F_r'\right). \tag{2.9}$$

Since terms like  $F_z''$  and  $F_z'$  are somewhat smaller in magnitude than  $F_r'$  and  $F_r$ , it follows that the ratio of the bending energy per unit area to  $\Omega$  is of the order of  $(t/a)^2$ . Thus, if the indentation radius is large compared to the film thickness the bending contribution to the elastic energy can be neglected.

### 3. Energy release rate for interfacial delamination

The indenter creates a free edge in the film at the radius  $r = a$  where it contacts the film. From this edge, where the film experiences the highest induced stresses, an interfacial crack between the film and the substrate may be initiated, spreading outward radially to the point where the energy release rate  $G$  available to drive the crack drops below the interface toughness. The interfacial delamination of the diamond film on the titanium substrate shown in figure 2 is accompanied by other phenomena, including buckling, cracking and break-up of the film at some distance

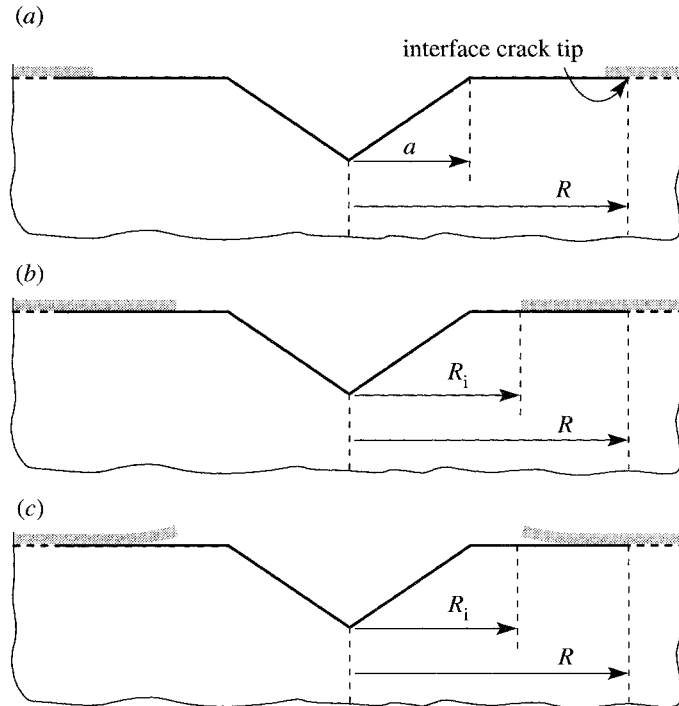


Figure 7. Models for interface delamination: (a) small annular plate of film remains with the most of films breaking up as the crack advances; (b) a substantial annular portion of the film remains without buckling as the crack advances; and (c) addition of buckling to (b).

behind the interface crack front. In this section, three models of the delamination process will be analysed and discussed giving insight and quantitative results on how these accompanying phenomena influence the energy release rate. The features of the three models are depicted in figure 7 and can be identified as follows.

(a) Delamination accompanied by break-up of the detached film such that a very narrow annular plate of film is left behind the advancing interface crack front.

(b) Delamination taking place with an unbuckled annular plate of film remaining intact behind the advancing interface crack front.

(c) As in (b) above, but with allowance for buckling of the annular plate of film.

(a) *Delamination leaving behind a very narrow annular plate of film*

The diamond film on the titanium substrate in figure 2 illustrates a case where the high residual compressive stress in the film causes detached portions of the film to buckle, crack and break-up leaving just a narrow annular plate of the film behind the interface crack tip. The interface crack spreads out radially until the energy release rate drops to the level of the interface toughness,  $\Gamma_c$ . Given the situation depicted in figure 7a, where a circular interface crack of radius  $R$  has only a very narrow annular strip of film behind it, the energy release rate  $G$  is given by

$$G = \frac{(1 - \nu^2)t}{2E} \sigma_r(R)^2, \quad (3.1)$$

where  $\sigma_r(R) = \sigma_0 + \sigma_r^I(R)$  denotes the combination of the initial residual stress and radial component of stress due to indentation in the attached film at  $r = R$ .

The argument for the validity of this formula is as follows. Delamination of a film of thickness  $t$  on an infinite substrate subject to a *uniform* stress  $\sigma$  due to steady-state advance of a *straight* interface crack is given by the well known expression  $G = (1 - \nu^2)t\sigma^2/(2E)$ , where  $\sigma$  acts perpendicular to the crack front. This is simply the difference between the elastic energies per unit area of the film when it is attached to the substrate and when it is released, subject to the condition of zero strain change parallel to the crack front. This result is independent of the component of residual stress in the film parallel to the crack front. In writing (3.1), the identification  $\sigma = \sigma_r(R)$  has been made under the assumption that the film thickness  $t$  is very small compared to the characteristic size of the indentation field, such that a 'local' condition of steady-state holds at the current crack front as an approximation. (It is noted again that the thickness of the diamond film in figure 2 is greater than  $a/500$ .) Secondly, if the annular region of detached film behind the advancing front is sufficiently narrow, the radial component of stress in the film behind the crack tip will be essentially zero such that the strain energy in the film will be released subject to zero strain change parallel to the crack front. Further insight into the effect of the width of the trailing strip of film will be given in the next sub-section. Finally, it is important to appreciate that the processes leading to the break-up of the film behind the advancing interface crack (buckling and film cracking) do not alter the validity of (3.1) for the crack at its current location.

The sign of  $\sigma_r$  determines the combination of mode I and mode II loading to which the interface crack is subject. If  $\sigma_r$  is tensile the magnitudes of the mode I and II stress intensity factors are about equal (Hutchinson & Suo 1991). However, if  $\sigma_r$  is compressive the interface behind the crack front is closed and mode II interface cracking occurs. Sufficiently near the indenter,  $\sigma_r$  is always compressive, and it is compressive for all  $R$  when the residual stress  $\sigma_0$  is compressive. However, when  $\sigma_0$  is tensile, there is a value of  $R$  where  $\sigma_r = 0$ , giving  $G = 0$  and marking a transition from mode II behaviour to mixed-mode behaviour. It is now well established that the toughness of many interfaces is strongly mode-dependent, and this has bearing on the relevant toughness quantity  $G_c$ . This issue will be addressed later in the paper.

In summary, the energy release rate of the interface crack at radius  $R$  with a very narrow strip of trailing film is given by (3.1). In the applications emphasized here,  $\sigma_r(R)$  will be negative such that the interface delamination is a mode II process. The radial component of stress in the film at  $r = R$  can be expressed in terms of the strains by

$$\sigma_r(R) = \left( \frac{E}{1 - \nu} \right) \varepsilon_0 + \frac{E}{(1 - \nu^2)} [\varepsilon_r^I(R) + \nu\varepsilon_\theta^I(R)] = \frac{E}{(1 - \nu^2)} [\varepsilon_r(R) + \nu\varepsilon_\theta(R)], \quad (3.2)$$

such that (3.1) becomes

$$\frac{G}{Et/(1 - \nu)} = \frac{1}{2(1 + \nu)} (\varepsilon_r(R) + \nu\varepsilon_\theta(R))^2. \quad (3.3)$$

Figure 8 gives plots of  $G/[Et/(1 - \nu)]$  as a function of  $R/a$  for the same set of parameters used in presenting  $\Omega$  in figure 5. For films with  $\varepsilon_0 \leq 0$ ,  $G$  falls monotonically to the level

$$G_0 = \frac{(1 - \nu^2)t}{2E} \sigma_0^2 = \frac{(1 + \nu)Et}{2(1 - \nu)} \varepsilon_0^2, \quad (3.4)$$

which corresponds to the energy release rate due to the residual stress remote from

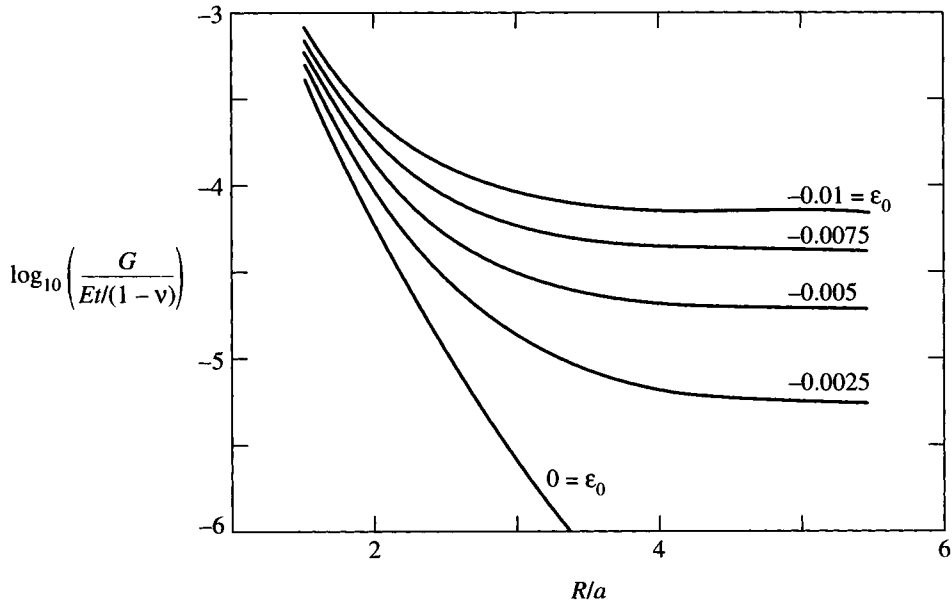


Figure 8. Normalized energy release rate as a function of compressive residual film strain and distance from the indentation for the model depicted in figure 7a.  $\nu = 0.3$ ,  $\sigma_Y/E_s = 0.005$  and  $N = 0.1$ .

the indenter. The stress induced by indentation dominates  $G$  for  $R$  less than about  $2a$ , and  $G$  approaches  $G_0$  for  $R$  greater than about  $5a$ , depending on  $\epsilon_0$ . Plots of  $G/G_0$  will be presented in §4 when application is made to predicting the toughness of the diamond–titanium interface. The strain hardening level of the substrate has a fairly strong influence on  $G$  as can be seen from the example in figure 9.

For completeness, curves for positive residual strain  $\epsilon_0$  are included in figure 10. When  $\epsilon_0 > 0$ ,  $G$  becomes zero at some intermediate radius  $R^*$  where  $\sigma_r(R^*) = 0$ ; at larger values of  $R$ ,  $\sigma_r(R)$  is positive and the crack is open behind the tip. When  $\epsilon_0 > 0$ , the interface crack would either arrest prior to reaching  $R^*$ .

(b) *Delamination with an unbuckled annular plate of film left behind the crack tip*

The film remaining within the circular delamination zone supplies a constraint which reduces the energy release rate. In this subsection, the effect on  $G$  of an annular plate of film with inner radius  $R_i$  will be determined, assuming the film does not buckle. Buckling reduces the constraint in the following subsection. The estimates of  $G$  obtained for the model analysed in this subsection are the lowest that can be expected.

The stress distribution in the annular plate of detached film is given by the Lamé’ solution, where the edge at the inner radius  $R_i$  is traction-free and the radial displacement at the outer edge at  $R$  is prescribed to be  $u = \epsilon_0 R + u^1(R) = R\epsilon_\theta(R)$ . The radial stress component at the outer edge of the annular plate is given by

$$\sigma_r(R^-) = \frac{E\epsilon_\theta(R)[1 - (R_i/R)^2]}{[(1 - \nu) + (1 + \nu)(R_i/R)^2]} \tag{3.5}$$

With  $\sigma_r(R)$  given by (3.2) as the stress in the attached film just outside the crack front,  $\Delta\sigma_r = \sigma_r(R) - \sigma_r(R^-)$  is the jump in the radial stress component in the film

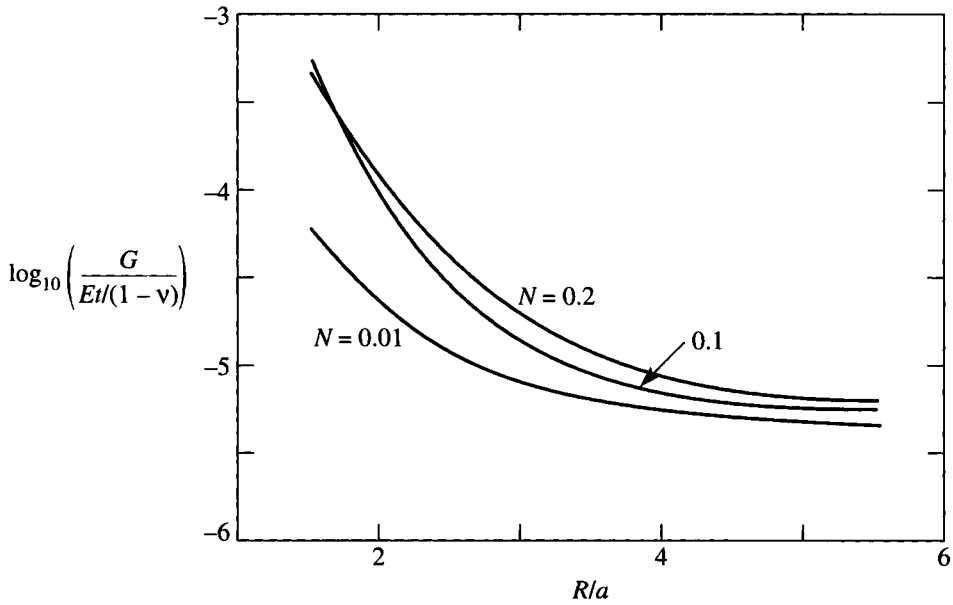


Figure 9. Effect of strain hardening on the normalized energy release rate for the advancing delamination crack for the model in figure 7a.  $\nu = 0.3$ ,  $\sigma_Y/E_s = 0.005$  and  $\epsilon_0 = -0.0025$ .

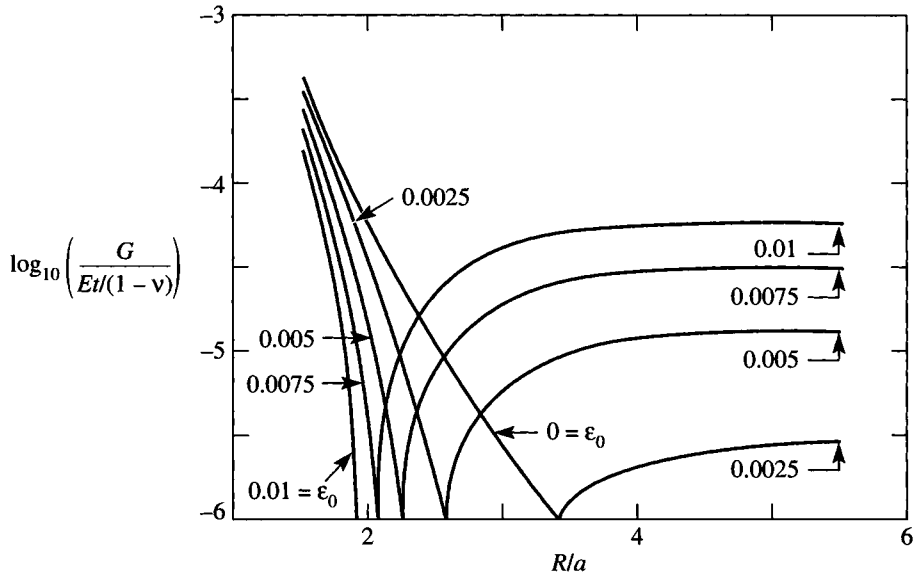


Figure 10. Normalized energy release rate as a function of tensile residual film strain for comparison with the behaviour of films under compressive strain in figure 8.  $\nu = 0.3$ ,  $\sigma_Y/E_s = 0.005$  and  $N = 0.1$ .

across the crack front. The energy release rate is still given by (3.1) but now with  $\sigma_r(R)$  replaced by  $\Delta\sigma_r$  giving

$$\frac{G}{Et/(1-\nu)} = \frac{1}{2(1+\nu)} \left( (\epsilon_r(R) + \nu\epsilon_\theta(R)) - \frac{(1-\nu^2)\epsilon_\theta(R)[1-(R_i/R)^2]}{[(1-\nu)(1+\nu)(R_i/R)^2]} \right)^2, \quad (3.6)$$

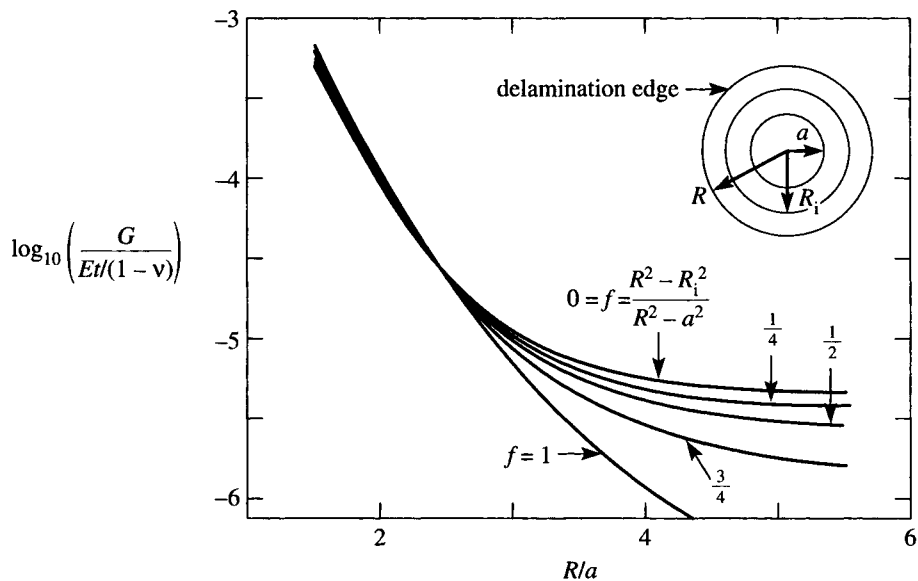


Figure 11. Normalized energy release rate for the annular film model depicted in figure 7b.  $\nu = 0.3$ ,  $N = 0.1$ ,  $\sigma_V/E_s = 0.005$  and  $\epsilon_0 = -0.0025$ .

where the strain quantities are those for the attached film at  $r = R$ . The primary interest here is for cases for which  $\Delta\sigma_r$  is negative, and, under this circumstance, the interface crack remains closed and propagates under mode II conditions.

Figure 11 illustrates the effect of the annular plate of unbuckled film on  $G$ . The case shown is one of those considered in figure 8 with  $\epsilon_0 = -0.0025$ , and the curve for  $R_i/R = 1$  ( $f = 0$ ) is the same as the corresponding curve in that figure. The curves in this figure are plotted for constant values of the ratio  $f$  of annular plate area to delamination area, i.e.

$$f = \frac{\pi(R^2 - R_i^2)}{\pi(R^2 - a^2)}. \tag{3.7}$$

The curve for a decohered film extending all the way back to the indentation (labeled by  $f = 1$ ) shows that the intact film results in a rapid drop-off of  $G$  for  $R$  greater than about  $2.5a$ . A circular delamination emanating from a circular region cut-out of film was used by Farris & Bauer (1988) to measure the interface toughness of thin films experiencing uniform residual biaxial tension. The present result in (3.6) reduces to this case in the absence of indentation strains such that  $\epsilon_r = \epsilon_\theta = \epsilon_0$ . In the presence of indentation, the case for  $f = 1$  is qualitatively similar, but complicated by the radial nonuniformity of the stresses in the film prior to delamination. The main conclusion to be drawn from figure 11 is that a relatively narrow annular region of intact film behind the interface crack front ( $f < \frac{1}{4}$ , say) has little effect on  $G$  such that (3.3) applies. Even the constraint offered by an annulus covering one half of the delaminated region results in a relatively small reduction of the energy release rate below (3.3).

(c) *Delamination with a buckled annular plate of film left behind the crack tip*

If the residual stress in the film is compressive, the stresses  $\sigma_r$  and  $\sigma_\theta$  in the annular plate of film left behind the delamination crack tip will be compressive. Consequently,



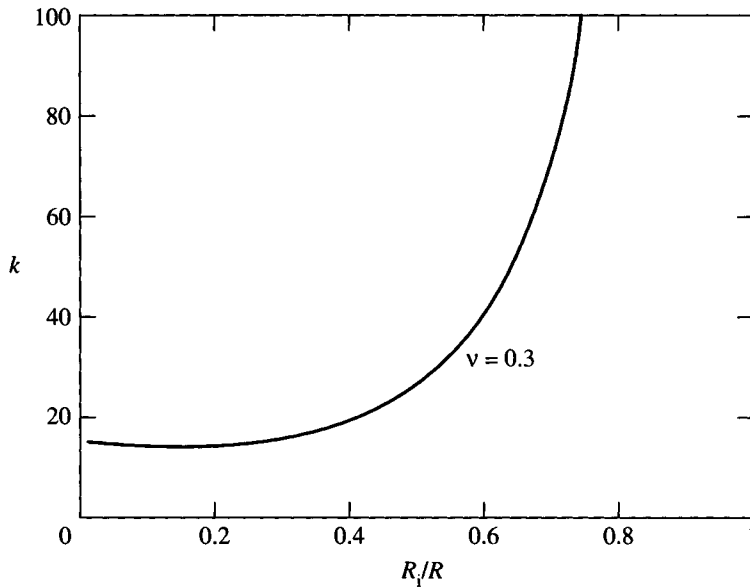


Figure 12.  $k$ -factor in the axisymmetric buckling analysis (3.9) of the annular film remaining behind the advancing delamination crack.

the plate may buckle and thereby reduce the constraint analysed in § 3 *b*. The effect of buckling, if it occurs, will be to increase the energy released relative to the prediction in § 3 *b*. Depending on the level of the compressive stresses and the area fraction  $f$ , the buckling mode can be either axisymmetric or non-axisymmetric, as is the case for the diamond film in figure 2. The distribution of  $\sigma_r$  in the unbuckled plate of film is

$$\sigma_r^0(r) = \sigma_r(R^-) \left( \frac{r - R_1}{R - R_1} \right), \quad (3.8)$$

where  $\sigma_r(R^-)$  is given by (3.5). For axisymmetric deformations, the linearized von Karman plate equations governing the critical conditions for axisymmetric buckling can be solved with a result in the form (Timoshenko & Gere 1961):

$$\sigma_r(R^-) = -k \left( \frac{R_1}{R}, \nu \right) \frac{E}{12(1 - \nu^2)} \left( \frac{t}{R} \right)^2, \quad (3.9)$$

where  $k$  is plotted in figure 12. The film will buckle depending on whether  $\sigma_r(R^-)$ , as given by (3.5), is larger or smaller in magnitude than the magnitude of the right hand of (3.9).

Under conditions in which (3.9) is exceeded, the plate will buckle away from the substrate simultaneously lowering the compressive membrane stress and inducing a bending moment at its outer edge. The effect is twofold. The energy release rate is increased due to the reduction in the constraint of the delaminated plate of film, and, if the bending moment is large enough, the interface crack tip will open giving rise to a mode I loading at the crack tip as well as a mode II contribution. Full details of these effects are given for the similar problem of buckling-driven delaminations studied by Hutchinson & Suo (1991) and Hutchinson *et al.* (1992). The effect of buckling on the indentation test will not be pursued in this paper because in most cases it is expected to lead to energy release rates which are even closer to  $G$  given by

(3.1) than those analysed in §3*b*. Moreover, the non-axisymmetric mode of buckling, which is more likely to occur than the axisymmetric mode when the annular region is narrow, is complicated by contact between the film and substrate over portions of the delaminated region. Insight into this behaviour can be obtained from the work of Thouless *et al.* (1994) on the problem of a straight edge-delamination of a biaxially compressed film on a substrate. Buckling due to compression parallel to the crack front is observed, accounting for alternating regions of contact and separation of the film and substrate. In regions along the front where the film buckles away from the substrate,  $G$  is enhanced and can exceed the value for edge delamination in (3.1).

In conclusion, buckling complicates delamination behaviour. Nevertheless, it reduces the constraining effect of the delaminated film and tends to drive the energy release rate towards the value (3.1) for unconstrained edge-delamination, or possibly even higher at points along the delamination front. There is some evidence in figure 2 that buckling of the annular strip remaining after delamination may have caused the interface crack front to depart locally from a circular shape, but the effect is small.

#### 4. Toughness of a diamond–titanium interface

Indentation-induced interface delamination is applied in this section to measure the toughness of a diamond-titanium alloy interface. A diamond coating was grown on substrates of a titanium alloy containing 6% Al and 4% V, commonly referred to as Ti-6Al-4V. Flat rectangular substrates of  $60 \times 20 \times 3 \text{ mm}^3$  dimensions were prepared for deposition by cleaning in solvents and scratching with a fine diamond powder to enhance nucleation. This pretreatment is commonly used to prepare samples for diamond growth by low pressure methods. Diamond deposition was performed in a chemical vapor deposition (CVD) reactor using microwave excitation at 2.45 GHz. Diamond film growth occurred under conditions of 1% methane in hydrogen with a total gas flow rate of  $200 \text{ std. cm}^3 \text{ min}^{-1}$  and a pressure of 80 torr. Growth proceeded until a film thickness of  $0.3\text{--}1.5 \text{ }\mu\text{m}$  was achieved, primarily by varying the growth time. The variation in film thickness allowed for the dependence of interface toughness with film thickness to be elucidated for the brale indentation test as elaborated on below. The presence of diamond was confirmed by Raman spectroscopy where a characteristic peak for diamond was observed which as significantly shifted to a value of  $1352 \text{ cm}^{-1}$  from  $1332 \text{ cm}^{-1}$  as a result of the residual compressive stresses in the film  $\sigma_0 = -7 \text{ GPa}$  (Ager & Drory 1993). Scanning electron microscopy was also performed where a fine-grained diamond coating of less than  $1 \text{ }\mu\text{m}$  grain size was observed (Drory & Hutchinson 1994).

The interface toughness was evaluated in this study by the Brale indentation method described in §1. Diamond-coated titanium coupons were indented over a range of 688, 1079 and 1570 N which are the preselected load values provided by the Rockwell Hardness Tester. The load is determined from the major loads derived from masses of 60, 100 and 150 kg added to the minor 10 kg preload. Values of the delamination radius,  $R/a$ , were measured in the optical microscope with side illumination to accentuate the delamination features. The film thickness was measured after indentation testing by imaging the delaminated film in the scanning electron microscope. Large increases in  $R/a$  for a given film thickness is caused by a higher indentation load. The data presented here provides the opportunity to combine experimental results with the mechanics analysis to give estimates of the diamond–titanium interface over a range of film thicknesses. Subsequent experimental work is needed to insure

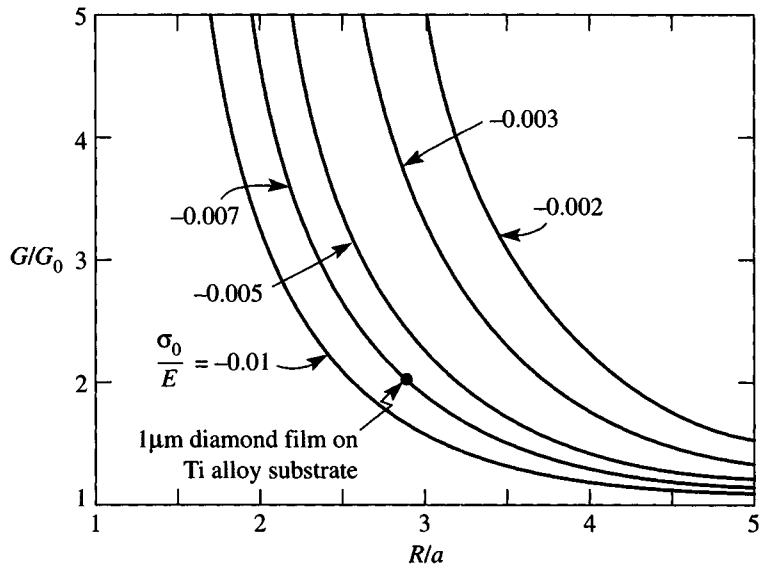


Figure 13. Trends in the normalized energy release rate with delamination radius as a function of compressive film stress. Present experiments on the diamond coated titanium alloy are indicated for a typical film thickness of  $1\ \mu\text{m}$ .  $\sigma_Y/E_s = 0.00792$ ,  $N = 0.05$ .

Table 3. Selected film and substrate material properties

property	diamond (Field 1992)	Ti-6Al-4V (ASM 1990)
yield stress, $\sigma_Y$ (MPa)	—	950
Young's modulus, $E$ (GPa)	1000	120
Poisson's ratio, $\nu$	0.07	0.36
work hardening coefficient, $N$	—	0.05

that the composition of the interface is comparable for each value of the interface toughness obtained. Initial work on the chemical analysis of the interface shows this to be a substantial task because of the difficulties in preparing specimens for analyses by scanning Auger microscopy and X-ray photoelectron spectroscopy (Perry *et al.* 1993).

Curves of  $G/G_0$  as a function of the ratio of the delamination radius to the indentation radius,  $R/a$ , based on (3.3) and (3.4) are plotted in figure 13 for the diamond film of thickness  $1\ \mu\text{m}$  and the titanium alloy substrate (cf. table 3). The curves are for various values of the compressive residual stress in the film, including that for the diamond film tested with  $\sigma_0 = -7\ \text{GPa}$  ( $\sigma_0/E = -0.007$ ). These results for the titanium alloy substrate with  $\sigma_Y/E_s = 0.00792$  and  $N = 0.05$  were obtained by linearly interpolating or extrapolating, as required, the results for  $F_r$  in (2.3) and table 2 for the values of  $\sigma_Y/E_s$  and  $N$  given. To illustrate the strong effect the substrate strain hardening index  $N$  has on the relation between  $G/G_0$  and the normalized delamination radius, similar plots are given in figure 14 with  $\sigma_0/E$  fixed at  $-0.007$  and  $\sigma_Y/E_s = 0.00792$  but with four values of  $N$ , ranging from a nearly perfectly plastic material to a high straining hardening material. It is seen in figures 13 and

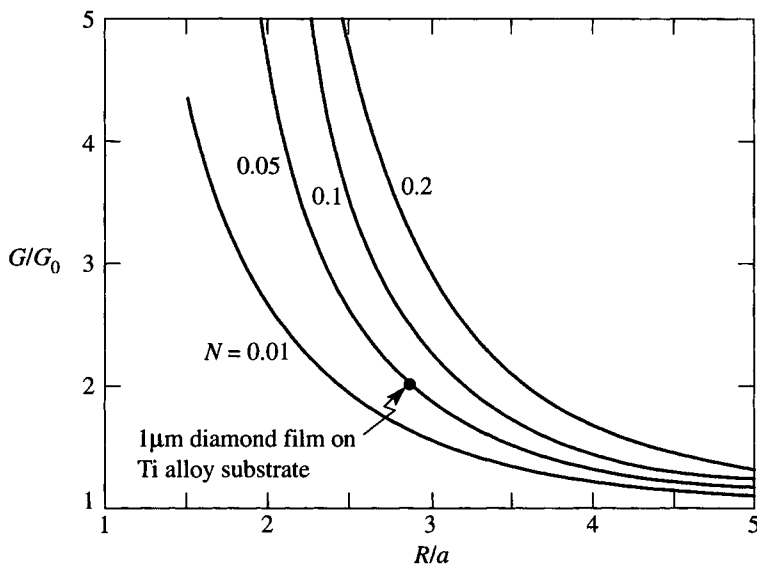


Figure 14. Variation in energy release rate as in figure 13, with the effect of substrate strain hardening.  $\sigma_Y/E_s = 0.00792$  and  $\sigma_0/E = -0.007$ .

14 that the energy release rate of the indentation-induced interface crack approaches the remote value  $G_0$  when  $R/a$  is on the order of 5 and is many times  $G_0$  when  $R/a$  is less than from 2 to 3, depending somewhat on  $N$  and  $\sigma_0/E$ . The useful range of the indentation test is when conditions are such that  $R/a$  lies between about 2 and 5. In this range, the value of  $G/G_0$  at a given  $R/a$  is much more sensitive to the strain hardening index  $N$  of the substrate than to its normalized yield stress  $\sigma_Y/E_s$ , and, consequently, the dependence on this latter parameter will not be shown here.

Figure 2 shows the delamination cracks for a  $1\ \mu\text{m}$  thick film for three indentation loads. The measured values of  $R/a$  for these and other tests are plotted in figure 15. At each film thickness  $t$  for which data is shown in figure 15, data is included for three indentation loads: 688, 1079 and 1570 N. The effect of the magnitude of the indentation load on  $R/a$  is small, consistent with the model of the test developed here for which the indentation radius enters only through  $R/a$ . For the diamond film of thickness  $t = 1\ \mu\text{m}$  supporting the compressive biaxial stress  $\sigma_0 = -7\ \text{GPa}$ , the elastic energy per unit area (2.7) and the energy release rate for edge delamination in the absence of indentation (3.4) are, respectively,

$$\Omega_0 = 45.6\ \text{J m}^{-2} \quad \text{and} \quad G_0 = 24.4\ \text{J m}^{-2}. \quad (4.1)$$

The measured value of  $R/a$  for films which are nominally  $1\ \mu\text{m}$  thick is approximately 2.85. A solid point corresponding to  $R/a = 2.85$  marking the curve in figures 13 and 14 for the diamond film on the titanium alloy substrate, indicates that the interface crack induced by the indenter arrested at a value of  $G/G_0 = 1.95$  or, by (4.1),  $G = 47.5\ \text{J m}^{-2}$ . The toughness of the interface,  $\Gamma_c$ , is identified with the value of  $G$  at which the crack arrests, and thus  $\Gamma_c = 47.5\ \text{J m}^{-2}$ . The arrest value of  $G$  obtained from (3.3) may be an overestimate but the error is expected to be small (cf. §3). As discussed in §3*a*, the interface crack advances under mode II conditions for compressed films undergoing edge delamination, and, accordingly,  $\Gamma_c$  should be regarded as the mode II toughness of the interface.

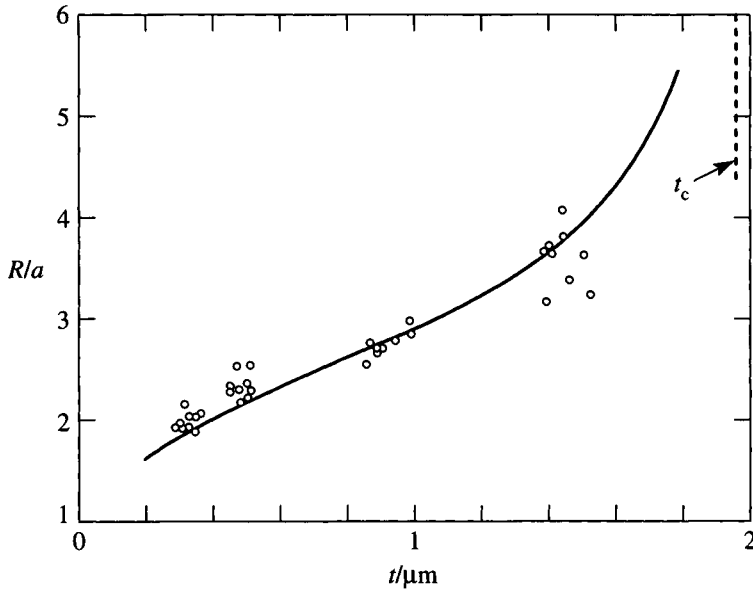


Figure 15. Normalized delamination radius *vs* film thickness for the diamond-coated titanium alloy. The solid line is the theoretical prediction based on  $\Gamma_c = 47.5 \text{ J m}^{-2}$  and the points are experimental values.  $\sigma_Y/E_s = 0.00792$ ,  $N = 0.05$ ,  $\sigma_0 = -7 \text{ GPa}$ .

The value of the interface toughness is many times the atomistic work of fracture of the interface and probably exceeds the toughness of the diamond film itself by at least a factor of two. Plastic deformation in the substrate almost certainly makes up a major portion of the interface toughness (Tvergaard & Hutchinson 1993). That the interface can be tougher than the film and still be the fracture path is a peculiarity of films in compression. Any crack-like flaws in the film tend to be closed by the residual stresses. Of course, once the film does become detached, it is susceptible to buckling and, therefore, tensile stresses due to bending. These tensile stresses can then cause the film to crack, as is evident in figure 2. Although extensive film cracking has obviously occurred, a simple estimate of the energy expended by this cracking reveals that it is very small compared to the energy consumed in delamination.

The solid line curve in figure 15 is the theoretical prediction of the normalized delamination radius,  $R/a$ , as a function of  $t$ . This prediction is obtained from (3.3) together with the criterion  $G = \Gamma_c$ , where  $\Gamma_c = 47.5 \text{ J m}^{-2}$  and  $\sigma_0 = -7 \text{ GPa}$  have been used. The solid points in the figure are data resulting from indentation tests on the diamond films with thicknesses ranging from about 0.3 to 1.5  $\mu\text{m}$ . The films with  $t = 1.5 \mu\text{m}$  display the most scatter in  $R/a$ , but, otherwise, the predicted trend of  $R/a$  with  $t$  follows the test data fairly faithfully. If edge cracking of the interface is initiated by any means, a film will completely detach from the substrate if  $G_0 \geq \Gamma_c$ . By (3.4), the critical thickness for complete detachment is (i.e.  $t$  such that  $G_0 = \Gamma_c$ )

$$t_c = \frac{2E\Gamma_c}{(1-\nu^2)\sigma_0^2}. \quad (4.2)$$

The critical film thickness for the present diamond–titanium system is  $t_c = 1.9 \mu\text{m}$ . This thickness is seen in figure 15 to be the limit at which the normalized delamination radius  $R/a$  becomes unbounded. Significant scatter in  $R/a$  is to be expected for films with thickness approaching  $t_c$ .

The authors thank N. A. Fleck, N. Ogbonna and Z. C. Xia for generating the numerical results for indentation of the substrate. The work of J.W.H. was supported in part by the National Science Foundation from grants MSS-92-02141 and DMR-94-00396 and in part by the Division of Applied Sciences at Harvard University. The work of M.D.D. was supported by the Air Force Materiel Command and the National Science Foundation under grant no. III-9360024.

## References

- Ager, J. W. III & Drory, M. D. 1993 Quantitative measurement of residual biaxial stress by Raman spectroscopy in diamond grown on a Ti alloy by chemical vapor deposition. *Phys. Rev. B* **48**, 2601–2607.
- ASM Handbook 1990 *Properties and selection: nonferrous alloys & special-purpose materials*, vol. 2. ASM International.
- ASTM 1994 E18–93 Standard test methods for Rockwell hardness and Rockwell superficial hardness of metallic materials. In *Annual book of ASTM standards*, vol. 03.01. Philadelphia, PA: ASTM.
- Bower, A. F., Fleck, N. A., Needleman, A. & Ogbonna, N. 1993 Indentation of a power law creeping solid. *Proc. R. Soc. Lond. A* **441**, 97–124.
- Charalambides, P. G., Lund, J., Evans, A. G. & McMeeking, R. M. 1989 Development of test method for measuring the mixed mode fracture resistance of bimaterial interfaces. *J. Appl. Phys.* **56**, 77–82.
- Dieter, G. E. 1986 *Mechanical metallurgy*, 3rd edn, p. 325. New York: McGraw–Hill.
- Drory, M. D., Gardinier, C. F. & Speck, J. S. 1991 Fracture toughness of chemically vapor-deposited diamond. *J. Am. Ceram.* **74**, 3148–3150.
- Drory, M. D. & Hutchinson, J. W. 1994 Diamond coating of titanium alloys. *Science* **263**, 1753–1755.
- Evans, A. G., Drory, M. D. & Hu, M. S. 1988 The cracking and decohesion of thin films. *J. Mat. Sci.* **3**, 1043–1049.
- Evans, A. G. & Hutchinson, J. W. 1984 On the mechanics of delamination and spalling in compressed films. *Int. J. Solids Structures* **20**, 455–466.
- Farris, R. J. & Bauer, C. L. 1988 A self-determination method of measuring the surface energy of adhesion coatings. *J. Adhesion* **26**, 293–300.
- Field, J. E. (ed.) 1992 *The properties of natural and synthetic diamond*. London: Academic.
- Gamlen, C. A., Case, E. D., Reinhard, D. K. & Huang, B. 1991 Adhesion of polycrystalline diamond thin films on single-crystal silicon substrates. *Appl. Phys. Lett.* **59**, 2529–2531.
- Hutchinson, J. W. & Suo, Z. 1991 Mixed mode cracking in layered materials. *Adv. Appl. Mech.* **29**, 63–191.
- Hutchinson, J. W., Thouless, M. D. & Liniger, E. G. 1992 Growth and configurational stability of circular buckling-driven film delaminations. *Acta metall. mater.* **40**, 295–308.
- Jensen, H. M., Hutchinson, J. W. & Kim, K.-S. 1990 Decohesion of a cut prestressed film on a substrate. *Int. J. Solids Structures* **26**, 1099–1114.
- Jindal, P. C., Quinto, D. T. & Wolfe, G. J. 1987 Adhesion measurements of chemically-vapor deposited and physically vapor deposited hard coatings on WC-Co substrates. *Thin Solid Films* **154**, 361–375.
- Kinloch, A. J., Lau, C. C. & Williams, J. G. 1994 The peeling of flexible laminates. *Int. J. Frac.* **66**, 45–70.
- Mehrotra, P. K. & Quinto, D. T. 1985 Techniques for evaluating mechanical properties of hard coatings. *J. Vac. Sci. Technol. A* **3**, 2401–2405.
- Perry, A. J. 1983 Scratch testing of hard coating. *Thin Solid Films* **107**, 167–180.
- Perry, S. S., Ager, J. W., Somorjai, G. A., McClelland, R. J. & Drory, M. D. 1993 Interface characterization of chemically vapor deposited diamond on titanium and Ti–6Al–4V. *J. Appl. Phys.* **74**, 7542–7550.
- Ritter, J. E., Lardner, T. J., Rosenfeld, L. & Lin, M. R. 1989 Measurement of adhesion of thin polymer coatings by indentation. *J. Appl. Phys.* **66**, 3626–3634.

- Sizemore, J., Hohlfelder, R. J., Vlassak, J. J. & Nix, W. D. 1995 Measuring the adhesion of diamond thin films to substrates using the blister test. *Mat. Res. Soc. Proc.* **383**, 197–207.
- Steinmann, P. A. & Hintermann, H. E. 1989 A review of the mechanical tests for assessment of thin-film adhesion. *J. Vac. Sci. Technol. A* **7**, 2267–2272.
- Thouless, M. D., Jensen, H. M. & Liniger, E. G. 1994 Delamination from edge flaws. *Proc. R. Soc. Lond. A* **447**, 271–279.
- Timoshenko, S. P. & Gere, J. M. 1961 *Theory of elastic stability*. New York: McGraw-Hill.
- Tvergaard, V. & Hutchinson, J. W. 1993 The influence of plasticity on mixed mode interface toughness. *J. Mech. Phys. Solids* **41**, 1119–1135.
- Yen, T.-Y., Kuo, C.-T. & Hsu, S. E. 1990 Adhesion of diamond films on various substrates. *Mat. Res. Soc. Symp. Proc.* **168**, 207–212.

*Received 14 July 1995; accepted 23 October 1995*